Available online at www.sciencedirect.com
ScienceDirect
Journal of Organometallic Chemistry 693 (2008) 1528–1535
Journal of Organometallic Chemistry
www.elsevier.com/locate/jorganchem

New triosmium–iridium clusters: Synthesis and molecular structure of $[Os_3Ir_2(Cp^*)_2(\mu\text{-}OH)(\mu\text{-}CO)_2(CO)_8Cl]$ (**1**), $[Os_3IrCp^*(\mu\text{-}OH)(CO)_{10}Cl]$ (**2**), $[Os_3IrCp^*(\mu\text{-}H)(\mu\text{-}Cl)(\eta^3,\mu_3\text{-}C_5H_2N(NH_2)Br)(CO)_9]$ (**3**) and $[Os_3IrCp^*(\mu\text{-}Cl)_2(\eta^2,\mu_3\text{-}C_5H_3N(NH)Br)(CO)_7]$ (**4**)

Yui-Bing Lee, Wing-Tak Wong *

Department of Chemistry, The University of Hong Kong, Pokfulam Road, Hong Kong, China

Received 25 September 2007; received in revised form 4 October 2007; accepted 4 October 2007
Available online 11 October 2007

This work is dedicated to Professor Frank Albert Cotton for his pioneering contributions to the chemistry of metal clusters.

Abstract

The trinuclear osmium carbonyl cluster, $[Os_3(CO)_{10}(MeCN)_2]$, is allowed to react with 1 equiv. of $[IrCp^*Cl_2]_2$ (Cp^* = pentamethylcyclopentadiene) in refluxing dichloromethane to give two new osmium–iridium mixed-metal clusters, $[Os_3Ir_2(Cp^*)_2(\mu\text{-}OH)(\mu\text{-}CO)_2(CO)_8Cl]$ (**1**) and $[Os_3IrCp^*(\mu\text{-}OH)(CO)_{10}Cl]$ (**2**), in moderate yields. In the presence of a pyridyl ligand, $[C_5H_3N(NH_2)Br]$, however, the products isolated are different. Two osmium–iridium clusters with different coordination modes of the pyridyl ligand are afforded, $[Os_3IrCp^*(\mu\text{-}H)(\mu\text{-}Cl)(\eta^3,\mu_3\text{-}C_5H_2N(NH_2)Br)(CO)_9]$ (**3**) and $[Os_3IrCp^*(\mu\text{-}Cl)_2(\eta^2,\mu_3\text{-}C_5H_3N(NH)Br)(CO)_7]$ (**4**). All of the new compounds are characterized by conventional spectroscopic methods, and their structures are determined by single-crystal X-ray diffraction analysis.

Keywords: Osmium; Iridium; Clusters; Pyridine

1. Introduction

The interest in mixed-metal clusters lies in the metal–metal bond that connects the two different core metal atoms, and mainly in their possible application in homogeneous and heterogeneous catalysis. The difference in the reactivity of the adjacent metal centers in mixed-metal clusters may provide additional bi- or multifunctional activation pathways and increase the selectivity of substrate–cluster interactions. It has been suggested that catalysis by mixed-metal clusters in a number of cases result in higher catalytic activity or different product selectivity than that observed for their homonuclear analogues [1,2]. Recently, they have also been shown to act as the precursors in the preparation of nanosized materials, which has aroused general interest in many different areas, including in electronic, industrial, and medical applications [3,4].

Different coordination modes of organic compounds can be observed in heterometallic clusters because of the possibility of metalloselectivity in ligand substitution and site selectivity, which in turn gives new insights into the possible coordination of organic compounds on bulk metal surfaces [5,6]. Iridium is well known for its high selectivity in many important industrial catalytic reactions [7,8]. It would be interesting to study whether the formation of mixed-metal clusters can further improve the catalytic activities and selectivity of the existing iridium catalysts.

* Corresponding author.
E-mail address: wtwong@hkucc.hku.hk (W.-T. Wong).

0022-328X/$ - see front matter © 2007 Elsevier B.V. All rights reserved.
doi:10.1016/j.jorganchem.2007.10.009

Mixed-metal clusters bearing cyclopentadienyl ligands have unique properties for ligand exchange reactions and coordination. This type of system has been well studied in osmium–rhodium clusters, with unique ligand substitution reactions and reactivities observed [9,10]. However, only a few studies have been published concerning this type of system in osmium–iridium mixed-metal clusters. The clusters can be prepared from the reaction of triosmium clusters and mononuclear iridium complexes that contain either Cp or Cp* [11–18]. Herein, we report the reaction of $[Os_3(CO)_{10}(MeCN)_2]$ with $[IrCp^*Cl_2]_2$ in refluxing dichloromethane, which gave rise to two new osmium–iridium mixed-metal clusters. In the presence of 2-amino-5-bromopyridine, however, another two new clusters, $[Os_3IrCp^*(\mu\text{-}H)(\mu\text{-}Cl)(\eta^3,\mu_3\text{-}C_5H_2N(NH_2)(CO)_9Br]$ (**3**) and $[Os_3IrCp^*(\mu\text{-}Cl)_2(\eta^2,\mu_3\text{-}C_5H_3N(NH)(CO)_7Br]$ (**4**), with different coordination modes of the ligand were afforded.

2. Results and discussion

2.1. Reaction of $[Os_3(CO)_{10}(MeCN)_2]$ with $[IrCp^*Cl_2]_2$

The triosmium carbonyl cluster, $[Os_3(CO)_{10}(MeCN)_2]$, was allowed to react with 1 equiv. of $[IrCp^*Cl_2]_2$ in refluxing dichloromethane to afford two new osmium–iridium mixed-metal clusters, $[Os_3Ir_2(Cp^*)_2(\mu\text{-}OH)(\mu\text{-}CO)_2(CO)_8Cl]$ (**1**) and $[Os_3IrCp^*(\mu\text{-}OH)(CO)_{10}Cl]$ (**2**), in moderate yields (Scheme 1). In its analogue reaction, however, $[IrCp^*(CO)_2]$ with $[Os_3(CO)_{10}(MeCN)_2]$ gives a trigonal Os_2Ir cluster, $[Os_2IrCp^*(CO)_9]$, and a tetrahedral Os_3Ir cluster, $[Os_3IrCp^*(CO)_{11}]$, as the major products [13].

The infrared spectra showed CO stretching bands for the terminal carbonyl ligands on **1** and **2**, whereas weak signals were observed for the bridging carbonyl vibrations for complex **1** at 1634 cm^{-1}. The ^1H NMR spectra of the complexes showed a singlet at 2.0–2.2 ppm, indicating the presence of η^5-terminally bound Cp* ligand. A broad singlet resonance at around 2.5 ppm was observed for the bridging hydroxyl groups on both complexes. The positive fast atom bombardment (FAB) mass spectra exhibited the molecular envelope at the m/z of the parent molecular ions, together with the daughter ion peaks due to the sequential loss of the carbonyl groups. The spectroscopic data (IR, ^1H NMR, and MS) of clusters **1** and **2** were fully consistent with their solid state structures, which were established by X-ray diffraction analysis.

Dark purple crystals of **1** suitable for structural analysis were grown by the slow evaporation of its saturated solution in CH_2Cl_2/*n*-hexane. The metal core of **1** bears a butterfly Os_3Ir core with a $[IrCp^*]$ group bound at one of the osmium atoms by two bridging carbonyl groups. The two triangular faces of the Os_3Ir butterfly have at a dihedral angle of 24.25°, with a hydroxyl group at one side. The valence electron count of this structure is 76, which is 2 electrons less than the prediction by the effective atomic number (EAN) rule. The average Ir–Os bond length observed in **1** is 2.802 Å, and is within the reported range of a typical Ir–Os bond (2.70–2.95 Å) [10–13]. The Ir(1) atom, however, does not lie on the same plane as the Os_3 triangular face, but at a distance of 1.002(1) Å above the plane. The Ir(2), Os(3), and the two bridging carbonyl ligands lie on the same plane, with a rather short Ir(2)–Os(3) bond length of 2.8276(8) Å compared to that of the carbonyl bridged metal–metal bond. The two carbonyl groups bridge the Ir(2)–Os(3) edge asymmetrically, with an average Ir(2)–C and Os(3)–C bond length of 2.135 Å and 1.985 Å, respectively. The difference in the bond lengths does not arise from the difference in metal radii, as the bond length of M–C in $[Ir_4(CO)_{12}]$ and $[Os_3(CO)_{12}]$ is 1.874 and 1.978 Å, respectively [19,20]. This structure is unique because this kind of metal–metal bond bridged by two carbonyl ligands on the same plane has not been reported in any osmium mixed-metal cluster. A bridging hydroxyl group is observed at one of the Os–Os edges, as confirmed by the ^1H NMR spectra. It bridges the metal center almost symmetrically, with the bond length of Os(1)–O(12) and Os(2)–O(12) at 2.09(2) and 2.12(1) Å, respectively. The oxygen atom, O(12), lies above

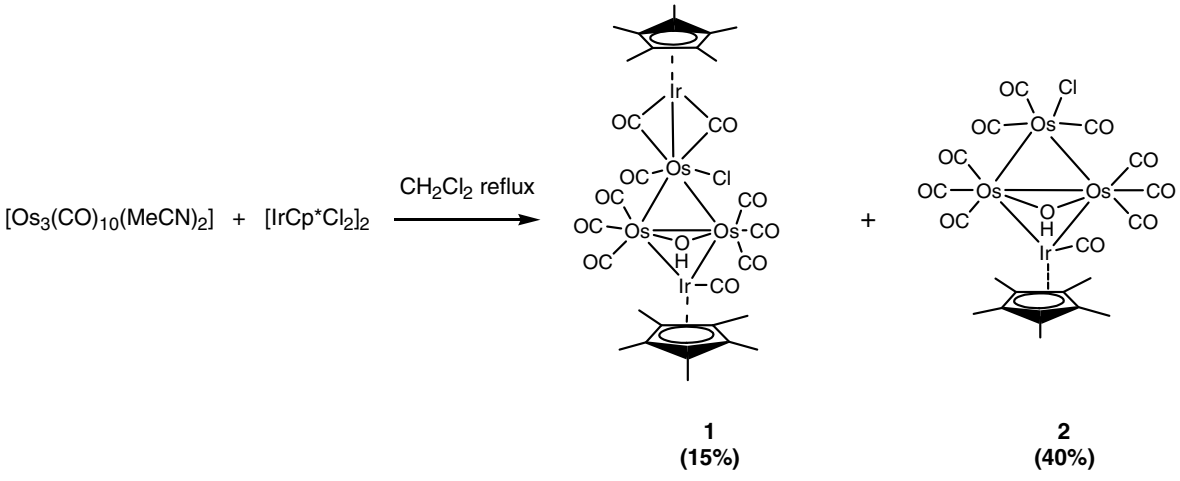

Scheme 1.

the basal plane of Os(1)Os(2)Os(3) at a distance of 1.600(9) Å. The O-bound hydrogen atom is located from the difference Fourier map and there is a restraint on the bond length of 0.82(1) Å. There is classical (O–H...Cl) H-bond interaction between the hydrogen atom on the hydroxyl group and the chloride ligand on Os(3) with a distance of 3.007 Å. The molecular structure of **1** and selected bond parameters are shown in Fig. 1 and Table 1, respectively.

Red crystals of **2** were obtained from the slow evaporation of its saturated solution in CH_2Cl_2/methanol for a week. Compound **2** possesses a butterfly Os_3Ir core with a dihedral angle of 19.374° between the two triangular faces, which is very similar to that of **1**. The valence electron count of the structure is 62, which is consistent with the prediction by the EAN. The average Ir–Os bond length observed in **2** is 2.783 Å, and is within the reported range of a typical Ir–Os bond. The average Os–Os bond is 2.792 Å, with an unusually short bond length of Os(1)–Os(2) of 2.6698(5) Å, whereas typically, the hydroxyl-bridged Os–Os bond has a range of 2.80–3.0 Å [21,22]. With the presence of a bridging hydroxyl group on the edge, the metal–metal bond tends to be elongated because of the steric hindrance of the group between the two metal atoms. This type of short metal–metal contact is rather rare in metal clusters with fewer than seven atoms, as it is generally agreed that the increase in nuclearity means that the bonding between the metal atoms becomes more metallic in character [23,24]. The Cp^* ligand is at an angle of 36.15° to the basal Os_3 plane and on the opposite side of the hydroxyl group. Similar to the case in cluster **1**, classical hydrogen bonding between the hydrogen atom of the hydroxyl group and the chloride ligand on Os(3) is observed in **2**, with a distance of 2.977 Å. The molecular structure of **2** and selected bond parameters are shown in Fig. 2 and Table 2, respectively.

Because of the highly similar Os_3Ir butterfly metal framework in clusters **1** and **2**, attempts were made to convert **2** to **1** by reacting it with one equivalent of $[(IrCp^*Cl_2)_2]$ in refluxing CH_2Cl_2, but no reaction was observed. The experiment was also repeated in high boiling solvents such as benzene, toluene, and heptane. However, no chemical change was observed after refluxing for 5 h.

Table 1
Selected bond lengths (Å) and angles (°) for $[Os_3Ir_2(Cp^*)_2(\mu\text{-OH})(\mu\text{-CO})_2(CO)_8Cl]$ (**1**)

Ir(1)–C(11)	1.81(2)	Ir(1)–Os(1)	2.777(1)
Ir(1)–Os(2)	2.801(1)	Ir(2)–C(19)	2.18(1)
Ir(2)–C(20)	2.09(1)	Ir(2)–Os(3)	2.8276(8)
Os(1)–O(12)	2.147(8)	Os(1)–Os(2)	2.700(1)
Os(1)–Os(3)	2.863(1)	Os(2)–O(12)	2.129(7)
Os(2)–Os(3)	2.8775(6)	Os(3)–C(19)	1.97(1)
Os(3)–C(20)	2.00(1)	Os(3)–Cl(1)	2.460(3)
Ir(1)–Os(1)–C(14)	160.7(4)	Ir(1)–Os(1)–Os(2)	61.49(3)
Ir(1)–Os(1)–Os(3)	119.10(4)	Ir(1)–Os(2)–Os(1)	60.63(3)
Ir(1)–Os(2)–Os(3)	117.83(4)	Ir(2)–C(19)–Os(3)	85.8(5)
Ir(2)–C(20)–Os(3)	87.3(4)	Ir(2)–Os(3)–C(19)	50.1(3)
Ir(2)–Os(3)–C(20)	47.6(3)	Ir(2)–Os(3)–Cl(1)	89.92(8)
Ir(2)–Os(3)–Os(1)	155.70(4)	Ir(2)–Os(3)–Os(2)	148.04(5)
Os(1)–Ir(1)–Os(2)	57.89(3)	Os(1)–O(12)–Os(2)	78.3(2)
Os(1)–Os(2)–Os(3)	61.69(2)	Os(1)–Os(3)–C(19)	105.7(3)
Os(1)–Os(3)–C(20)	156.6(3)	Os(1)–Os(3)–Cl(1)	87.75(8)
Os(1)–Os(3)–Os(2)	56.10(2)	Os(2)–Os(1)–Os(3)	62.22(2)
Os(2)–Os(3)–C(19)	161.8(3)	Os(2)–Os(3)–C(20)	100.9(3)
Os(2)–Os(3)–Cl(1)	88.55(8)	Os(3)–Ir(2)–C(19)	44.1(3)
Os(3)–Ir(2)–C(20)	45.1(3)		

2.2. Reaction of $[Os_3(CO)_{10}(MeCN)_2]$ with $[IrCp^*Cl_2]_2$ in the presence of 2-amino-5-bromopyridine

To study the coordination of a bidentate ligand on a mixed-metal system, the experiment was repeated with the presence of diaminoalkyls, pyrazole, pyrazine, 2-aminopyridine, and 2-amino-5-bromopyridine. However, no substituted osmium–iridium mixed-metal clusters could be isolated, except in the case of 2-amino-5-bromopyridine. Two new clusters $[Os_3IrCp^*(\mu\text{-H})(\mu\text{-Cl})(\eta^3,\mu_3\text{-}C_5H_2N\text{-}$

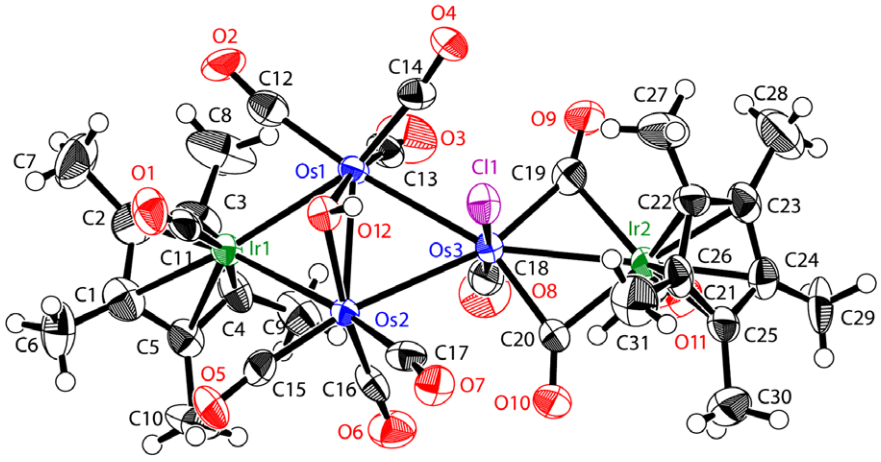

Fig. 1. ORTEP drawing (ellipsoids shown at 50% probability) of **1**, with the atomic labeling system (labels for the organic hydrogen atoms are omitted for clarity).

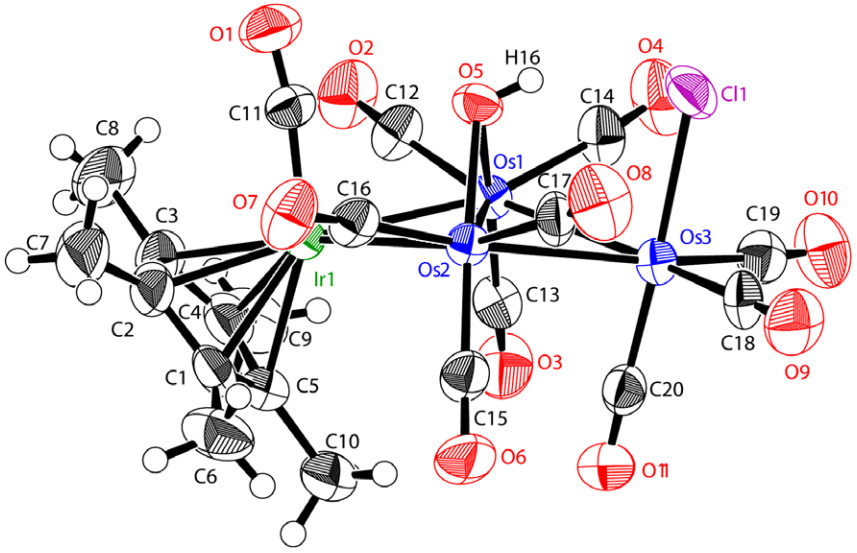

Fig. 2. ORTEP drawing (ellipsoids shown at 50% probability) of **2**, with the atomic labeling system (labels for the organic hydrogen atoms are omitted for clarity).

Table 2
Selected bond lengths (Å) and angles (°) for $[Os_3(IrCp^*)(\mu\text{–}OH)(CO)_{10}(Cl)]$ (**2**)

Ir(1)–Os(1)	2.7939(5)	Ir(1)–Os(2)	2.7719(5)
Os(1)–Os(2)	2.6698(5)	Os(1)–Os(3)	2.8577(5)
Os(1)–O(5)	2.113(6)	Os(2)–O(5)	2.130(6)
Os(2)–Os(3)	2.8496(5)	Os(3)–Cl(1)	2.467(2)
Os(1)–Ir(1)–Os(2)	57.32(1)	Ir(1)–Os(1)–Os(2)	60.92(1)
Ir(1)–Os(1)–Os(3)	119.94(2)	Os(2)–Os(1)–Os(3)	61.96(1)
Ir(1)–Os(2)–Os(1)	61.75(1)	Ir(1)–Os(2)–Os(3)	121.02(2)
Os(1)–Os(2)–Os(3)	62.26(1)	Os(1)–O(5)–Os(2)	78.0(2)

$(NH_2)(CO)_9Br]$ (**3**) and $[Os_3IrCp^*(\mu\text{-}Cl)_2(\eta^2, \mu_3\text{-}C_5H_3N\text{-}(NH)(CO)_7Br]$ (**4**), with different coordination modes of the ligand were afforded in the reaction, but neither cluster **1** nor **2** could be isolated (Scheme 2).

The infrared spectra showed that only terminal carbonyl ligands were observed in **3** and **4**, as C–O stretching bands lie within the range of 1950–2250 cm^{-1}. The ^1H NMR spectra of both complexes showed a singlet at 2.0–2.2 ppm, indicating the presence of a η^5-terminally bound Cp^* ligand. The ^1H NMR spectra of **3** exhibited two doublets ($\delta = 8.96$ and 8.24) assigned to the pyridyl protons. A broad weak signal was observed at $\delta = 4.37$

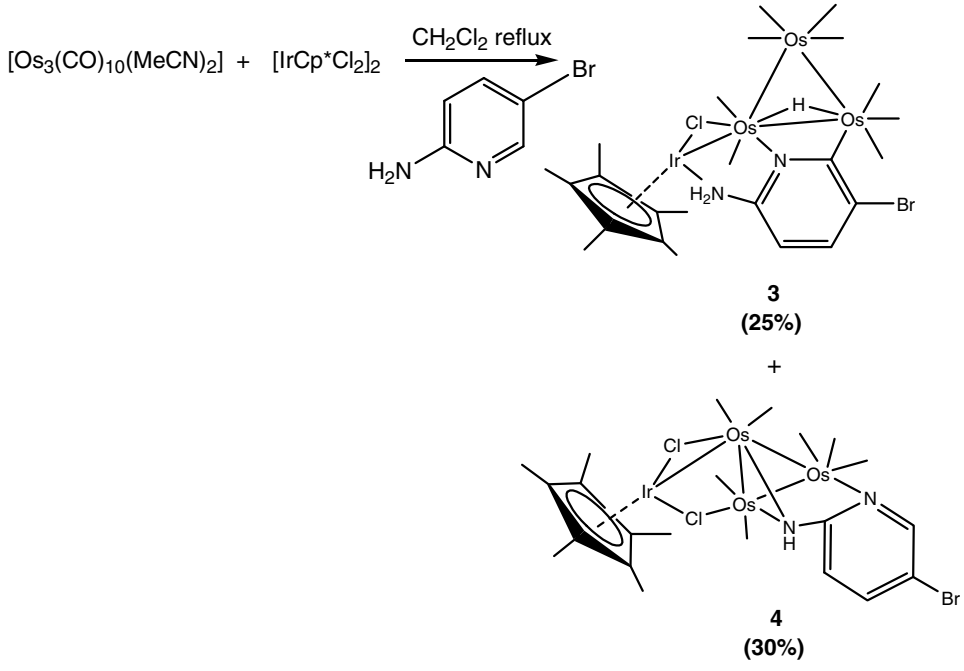

Scheme 2.

for the hydrogen atoms on the amino group. Singlet sharp hydride resonance was observed at $\delta = -17.85$. The ^{1}H NMR spectra of **4**, however, exhibited three multiplets ($\delta = 8.72$, 8.10, and 7.54) assigned to the three pyridyl protons. A broad weak signal was also observed at $\delta = 4.57$ for the hydrogen atom on the amino group. This suggests that the coordination mode of the pyridyl ligand is different for the two clusters. The positive fast atom bombardment (FAB) mass spectra exhibited the molecular envelope at the m/z of the parent molecular ions, together with the daughter ion peaks, because of the sequential loss of the carbonyl groups. The spectroscopic data (IR, ^{1}H NMR, and MS) of clusters **3** and **4** were fully consistent with their solid state structures, which were established by X-ray diffraction analysis.

Blue crystals of **3** were obtained from the slow evaporation of its saturated solution in CH_2Cl_2/methanol for a week. The solid state structure of **3** consists of a triangular Os_3 core with an [IrCp*] unit bounded by a bridging chloride ligand. The amino group of 2-amino-5-bromopyridine is bound to the iridium center with an Ir–N bond distance of 2.052(6) Å, which is comparable to a typical Ir-amino bond [25]. The nitrogen atom and the ortho-carbon atom of the pyridine are bound to two osmium centers at a bond length of 2.100(6) and 2.12(1) Å, respectively. The pyridyl ligand bonds at the axial position of the osmium atoms, with a dihedral angle observed between the planar pyridyl ligand and the Os_3 triangular face equals to 72.2°. It is rarely observed that this kind of ligand serves as a tridentate ligand bridging across three metal centers, with orthometallation taking place. Similar orthometallation of the pyridyl ligand has been observed in another triosmium cluster, $[Os_3(CO)_{10}(\eta^2,\mu\text{-}NC_5H_3N{=}NOPh)]$, with a comparable Os–C bond length (Os–C 2.108 Å) [26]. The valence electron count of this structure is 62, which is consistent with the prediction by the EAN. The Ir–Os bond length observed in **3** is 2.7760(5) Å, and is shorter than our prediction as it is bridged by a bulky chloride atom. The average Os–Os bond is 2.8797 Å, which falls within the range of a typical Os–Os bond [$Os_3(CO)_{12}$ 2.877(3) Å] [19]. A hydride signal was observed in the ^{1}H NMR spectrum, and is located at the Os(1)–Os(2) edge as it has a longer bond length (2.9578(4) Å) than the other Os–Os edges, and falls within the range of hydride-bridged Os–Os bonds. The molecular structure of **3** and selected bond parameters are shown in Fig. 3 and Table 3, respectively.

Red crystals of **4** were obtained from the slow evaporation of a saturated solution in CH_2Cl_2/methanol for a week. The solid state structure of **4** consists of a triangular Os_3 core with an IrCp* unit bounded by two bridging chloride ligands. A different coordination mode for the pyridyl ligand is observed in **4**, i.e., it acts as a bidentate ligand, bridging over three osmium atoms. A similar coordination mode of the aminopyridyl ligand has been observed for a triosmium cluster, $[Os_3(CO)_{10}(\eta^2,\mu_3\text{-}C_5H_4N_2Ph)]$ [27]. The two chloride ligands bridge the Ir center and Os center asymmetrically, with shorter Ir–Cl bond lengths observed

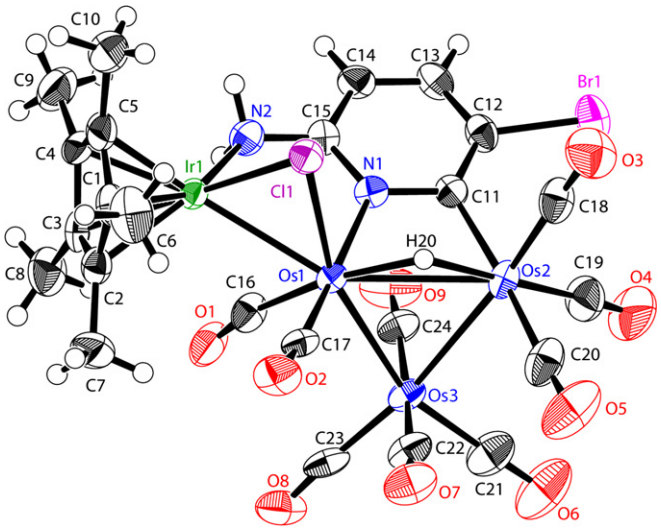

Fig. 3. ORTEP drawing (ellipsoids shown at 50% probability) of **3**, with the atomic labeling system (labels for the organic hydrogen atoms are omitted for clarity).

Table 3
Selected bond lengths (Å) and angles (°) for $[Os_3IrCp^*(\mu\text{-}H)(\mu\text{-}Cl)(\eta^3,\mu_3\text{-}C_5H_2N(NH_2)Br)(CO)_9]$ (**3**)

Ir(1)–Os(1)	2.7760(5)	Ir(1)–N(2)	2.052(6)
Os(1)–Os(2)	2.9578(4)	Os(1)–Os(3)	2.8181(5)
Os(1)–Cl(1)	2.543(2)	Os(1)–N(1)	2.100(6)
Os(2)–Os(3)	2.8632(6)	Os(2)–C(11)	2.12(1)
Cl(1)–Os(2)–N(1)	82.1(3)	Cl(2)–Os(1)–N(1)	84.0(3)
Ir(1)–Cl(1)–Os(2)	78.27(9)	Ir(1)–Cl(2)–Os(1)	76.2(1)
Os(1)–N(1)–C(18)	115.3(8)	Os(1)–N(1)–Os(2)	84.2(3)
Os(1)–Os(2)–N(1)	48.0(2)	Os(1)–Os(2)–Os(3)	58.10 (2)
Os(1)–Os(3)–N(2)	82.1(2)	Os(1)–Os(3)–Os(2)	63.94(2)
Os(2)–Os(1)–Cl(2)	97.73(7)	Os(2)–Os(1)–N(1)	47.9(2)
Os(2)–Os(1)–Os(3)	57.96(2)	Os(2)–Os(3)–N(2)	82.7(3)
Os(3)–Os(1)–Cl(2)	155.04(8)	Os(3)–Os(1)–N(1)	75.3(2)
Os(3)–Os(2)–N(1)	75.4(2)		

(average Ir–Cl = 2.428 Å, Os–Cl = 2.539 Å). However, direct bonding is observed only between Ir(1) and Os(1), with an elongated bond length of 3.0528(6) Å, whereas the distance between Ir(1) and Os(2) is 3.1484(7) Å. The average Os-Os bond length observed is 2.7923 Å, with the longer Os(1)–Os(2) bond due to the steric hindrance from the bridging pyridyl group (Os(1)–Os(2) 2.8998(7) Å). The average Os–N bond observed is 2.163 Å, which is comparable to that of $[Os_3(CO)_{10}(\eta^2,\mu_3\text{-}C_5H_4N_2Ph)]$ [27]. The ORTEP drawing of the molecular structure of **4** and selected bond parameters are shown in Fig. 4 and Table 4, respectively.

Although a triosmium cluster with substituted pyridine ligands can be prepared by reacting the pyridine ligand with $[Os_3(CO)_{10}(MeCN)_2]$ in the presence of a decarbonylating agent, no triosmium cluster substituted by 2-amino-5-bromopyidine could be isolated in our reaction.

Reactions were also effected to study whether the iridium complex is added to the triosmium cluster prior to

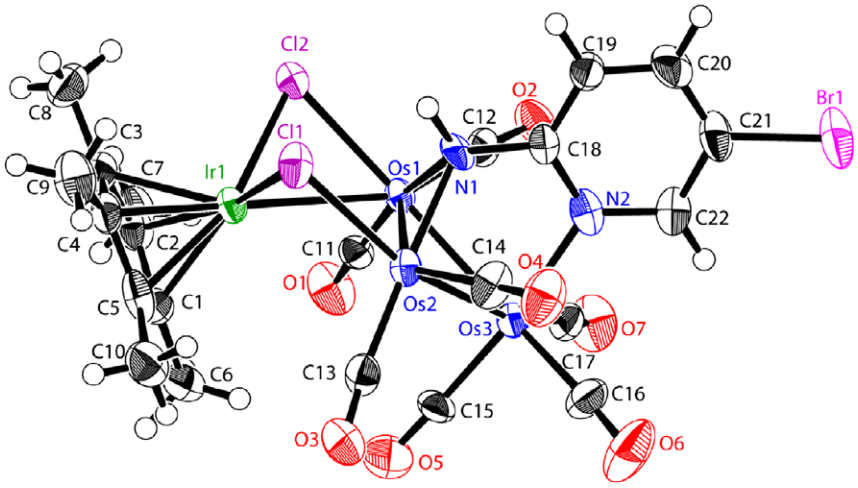

Fig. 4. ORTEP drawing (ellipsoids shown at 50% probability) of **4**, with the atomic labeling system (labels for the organic hydrogen atoms are omitted for clarity).

Table 4
Selected bond lengths (Å) and angles (°) for $[Os_3IrCp^*(\mu\text{–}Cl)_2(\eta^2,\mu_3\text{-}C_5H_3N(NH)Br)(CO)_7]$ (**4**)

Ir(1)–Cl(1)	2.434(3)	Ir(1)–Cl(2)	2.422(3)
Ir(1)–Os(1)	3.0528 (6)	Os(1)–Os(2)	2.8998(7)
Os(1)–Os(3)	2.7407(7)	Os(1)–Cl(2)	2.525(3)
Os(2)–Cl(1)	2.553(3)	Os(2)–Os(3)	2.7364(6)
Os(1)–N(1)	2.166(9)	Os(2)–N(1)	2.16(1)
Os(3)–N(2)	2.17(1)		
Cl(1)–Ir(1)–Cl(2)	89.7(1)	Cl(2)–Os(1)–N(1)	84.0(3)
Ir(1)–Cl(1)–Os(2)	78.27(9)	Ir(1)–Cl(2)–Os(1)	76.2(1)
Os(1)–N(1)–Os(2)	84.2(3)	Os(1)–Os(2)–Cl(1)	94.12(8)
Os(1)–Os(2)–N(1)	48.0(2)	Os(1)–Os(2)–Os(3)	58.10(2)
Os(1)–Os(3)–Os(2)	63.94(2)	Os(2)–Os(1)–Os(3)	57.96(2)
Os(3)–Os(1)–Cl(2)	155.04(8)	Os(3)–Os(1)–N(1)	75.3(2)
Os(3)–Os(2)–Cl(1)	151.81(8)	Os(3)–Os(2)–N(1)	75.4(2)

the substitution of the carbonyl ligands by the pyridyl group. Both complex **1** and **2** were allowed to react with an excess of 2-amino-5-brompyridine in a refluxing CH_2Cl_2 solution, but they remained unreacted after five hours.

3. Conclusion

Two osmium–iridium mixed-metal clusters (**1** and **2**) were afforded from the reaction of $[Os_3(CO)_{10}(MeCN)_2]$ with $[IrCp^*Cl_2]_2$. The reaction also took place in the presence of 2-amino-5-bromopyridine, but two other osmium–iridium clusters (**3** and **4**) with different coordination modes of the ligand were afforded.

4. Experiments

4.1. General procedures

All reactions were carried out under an atmosphere of dried and purified nitrogen gas using the standard Schlenk technique. The solvents used were distilled from appropriate drying agents and freshly prepared before use. Routine separation of products was performed by thin-layer chromatography (TLC) using 20 cm × 20 cm glass plates, coated with a 0.5 mm thickness of Merck Keiselgel 60 PF_{254}. Infrared spectra were recorded in a dichloromethane solution on a Bio-rad FTS-7 IR spectrometer using 0.5 mm CaF_2 solution cells, unless otherwise stated. ^1H NMR spectra were recorded on a Bruker DPX-400 NMR spectrometer using CD_2Cl_2 and referenced to $SiMe_4$ ($\delta = 0$). Positive ionization fast atom bombardment (FAB) mass spectra were recorded on a Finnigan MAT 95 mass spectrometer, using 3-nitrobenzyl alcohol as the matrix solvent. The starting materials, $[Os_3(CO)_{10}(MeCN)_2]$ [28] and $[IrCp^*Cl_2]_2$ [29], were prepared according to procedures detailed in the literature. 2-amino-5-bromopyidine was purchased from Aldrich and used directly without further purification.

4.2. Reaction of $[Os_3(CO)_{10}(MeCN)_2]$ and $[IrCp^*Cl_2]_2$

$[Os_3CO)_{10}(MeCN)_2]$ (50 mg, 0.057 mmol) and $[IrCp^*Cl_2]_2$ (21.3 mg, 0.057 mmol) were refluxed in CH_2Cl_2 for 4 h. The solution was allowed to cool, and the solvent was removed under vacuum. The mixture was then separated by TLC using the eluent of dichloromethane/hexane in a ratio of 3:7. A purple band and red band were isolated in order of elution as **1** ($R_f = 0.35$, 15%) and **2** ($R_f = 0.5$, 40%). Anal. Calc. for **1**: C, 23.47; H, 1.97. Found: C, 23.50; H, 1.96%. Anal. Calc. for **2**:C, 19.50; H, 1.31. Found: C, 19.52; H, 1.30%.

4.3. Reaction of $[Os_3(CO)_{10}(MeCN)_2]$ and $[IrCp^*Cl_2]_2$ in the presence of 2-amino-5-bromopyridine

Into the CH_2Cl_2 solution of $[Os_3CO)_{10}(MeCN)_2]$ (50 mg, 0.057 mmol) and $[C_5H_3N(NH_2)Br]$ (10.8 mg, 0.063 mmol), $[IrCp^*Cl_2]_2$ (21.3 mg, 0.057 mmol) was

Table 5
Spectroscopic data for complexes **1**–**4**

Compound	IR (ν_{CO})[a] (cm^{-1})	^1H NMR[b] (ppm)	MS[c] (*m*/*z*)
1	1634w, 1981m, 2008s, 2019s, 2039m, 2052m, 2071m	2.04 [s, 15H, Cp*] 1.98 [s, 15H, Cp*] 2.5 [br, 1H, OH]	1586 (1586.0)
2	2002m, 2033s, 2068m, 2087m	2.11 [s, 15H, Cp*] 2.5 [br, 1H, OH]	1232 (1231.9)
3	1962s, 1991m, 2023s, 2033s, 2054m, 2066w, 2083w	2.21 [s, 15H, Cp*] 4.37 [s, 2H, N–H] 8.96 [d, 1H] 8.24 [d, 1H] −17.85 [s, 1H]	1359 (1358.8)
4	1979m, 1996m, 2019m, 2050m, 2067s, 2085m	2.19 [s, 15H, Cp*] 4.57 [s, 1H, N–H] 7.54 [m, 1H] 8.10 [m, 1H] 8.72 [m, 1H]	1337 (1336.8)

[a] Recorded in CH_2Cl_2.
[b] Recorded in CD_2Cl_2 at 298 K.
[c] Positive FAB MS, calculated values in parentheses.

Table 6
Crystallographic data and data collection parameters of complexes **1**–**4**

Complex	**1**	**2**	**3**	**4**
Empirical formula	$C_{31}H_{31}ClIr_2O_{12}Os_3$	$C_{20}H_{16}ClIrO_{11}Os_3$	$C_{24}H_{20}BrClN_2IrO_9\ Os_3$	$C_{22}H_{19}BrCl_2N_2IrO_7Os_3$
Formula weight	1586.07	1230.61	1358.61	1337.03
Crystal system	Monoclinic	Monoclinic	Monoclinic	Monoclinic
Space group	*Pn*(#7)	$P2_1/n$ (#14)	$P2_1/n$ (#14)	$P2_1/n$(#14)
a (Å)	8.956(2)	8.887(2)	19.058(2)	9.234(1)
b (Å)	14.436(2)	20.029(4)	8.666(1)	23.332(3)
c (Å)	14.206(2)	15.091(3)	19.996(2)	13.484(2)
α (°)	90	90	90	90
β (°)	93.396(3)	92.456(4)	114.590(2)	90.794(2)
γ (°)	90	90	90	90
V ($Å^3$)	1833.4(5)	2683.7(9)	3003.2(6)	2904.8(7)
Z	2	4	4	4
D_{calc} (Mg/m^3)	2.873	3.046	3.005	3.057
F(000)	1424.00	2184.00	2428.00	2380.00
Crystal size (mm^3)	$0.02 \times 0.05 \times 0.18$	$0.02 \times 0.04 \times 0.10$	$0.03 \times 0.08 \times 0.20$	$0.04 \times 0.16 \times 0.48$
Reflections collected	6482	6139	6852	6629
[R_{int}]	0.049	0.072	0.065	0.106
Maximum and minimum transmission	0.491, 0.701	0.247, 0.680	0.382, 0.573	0.112, 0.463
Goodness-of-fit on F^2	1.039	1.025	1.087	1.022
Final *R* indices [$I > 2\sigma(I)$]	$R_1 = 0.028$, $wR_2 = 0.029$	$R_1 = 0.0366$, $wR_2 = 0.0375$	$R_1 = 0.0316$, $wR_2 = 0.0382$	$R_1 = 0.050$, $wR_2 = 0.0655$
Residual extrema in the final ΔF map (e $Å^{-3}$)	2.37, −1.64	1.58, −3.54	1.85, −1.94	2.78, −4.32

added. The solution was allowed to reflux for 4 h. It was then cooled to room temperature, and the solvent was removed under vacuum. The mixture was then separated by TLC using the eluent of dichloromethane/*n*-hexane in a ratio of 3:7. A red band and blue band were isolated in order of elution as **3** ($R_f = 0.3$, 25%) and **4** ($R_f = 0.6$, 30%). Anal. Calc. for **3**: C, 21.21; H, 1.48; N, 2.06. Found: C, 21.20; H, 1.50; N, 2.05%. Anal. Calc. for **4**: C, 19.77; H, 1.43; N, 2.10. Found: C, 19.75; H, 1.40; N, 2.15%. (see Table 5).

5. X-ray crystal structure determinations

All pertinent crystallographic data are summarized in Table 6. Crystals suitable for X-ray analyses were glued on glass fibers with epoxy resin or sealed in a 0.3 mm glass capillary. Intensity data for **1**, **2**, **3**, and **4** were collected at an ambient temperature on a Bruker AXS SMART 1000 CCD area detector with graphite monochromated Mo Kα radiation ($\lambda = 0.71073$ Å), operated at 50 kV and 30 mA. All structures were solved by direct methods and

expanded by difference Fourier maps. All metal atoms were refined anisotropically. Hydrogen atoms were generated at their idealized positions with C–H = 0.95 Å, and were included in the structure factor calculations using the riding model with $U_{iso}(H) = 1.2\ U_{eq}(C)$. Hydrides were placed at their ideal positions as determined by the positions of the equatorial carbonyl ligands, but were not refined.

Acknowledgements

We gratefully acknowledge the financial support provided by the Research Grants Council of Hong Kong and the University of Hong Kong. Y.-B. Lee acknowledges the receipt of a postgraduate studentship (2004–2008) administrated by the University of Hong Kong.

Appendix A. Supplementary material

CCDC 659721, 659722, 659723 and 659724 contain the supplementary crystallographic data for this paper. These data can be obtained free of charge from The Cambridge Crystallographic Data Centre via www.ccdc.cam.ac.uk/data_request/cif. Supplementary data associated with this article can be found, in the online version, at doi:10.1016/j.jorganchem.2007.10.009.

References

[1] F.W. Vergeer, M. Lutz, A.L. Spek, M.J. Calhorda, D.J. Stufkens, F. Hartl, Eur. J. Inorg. Chem. (2005) 2206.
[2] D.J. Dyson, Coord. Chem. Rev. 248 (2004) 2443.
[3] P. Jena, S.N. Khanna, B.K. Rao, Clusters and Nano-assemblies: Physical and Biological Systems, Richmond, Virginia, USA, 2003.
[4] M.W. DeGroot, H. Rosner, J.F. Corrigan, Chem. Eur. J. 12 (2006) 1547.
[5] J.A. Cabeza, I. del Rio, V. Riera, M. Suarez, Organometallics 23 (2004) 1107.
[6] J.A. Cabeza, I. del Rio, V. Riera, M. Suarez, Organometallics 21 (2002) 2540.
[7] A. Izumi, Y. Obora, S. Sakaguchi, Y. Ishii, Tetrahedron Lett. 47 (2006) 9199.
[8] Y.-Y. Li, X.-Q. Zhang, Z.-R. Dong, W.-Y. Shen, G. Chen, J.-X. Gao, Org. Lett. 8 (2006) 5565.
[9] S.Y.-W. Hung, W.-T. Wong, J. Organomet. Chem. 580 (1999) 48.
[10] J.P.-K. Lau, W.-T. Wong, Inorg. Chem. Commun. 6 (2003) 733.
[11] P. Srinivasan, J. Tan, W.K. Leong, J. Organomet. Chem. 691 (2006) 1288.
[12] P. Srinivasan, W.K. Leong, J. Organomet. Chem. 691 (2006) 403.
[13] A. Riesen, F.W.B. Einstein, A.K. Ma, P.K. Pomeroy, J.A. Shipley, Organometallics 10 (1991) 3629.
[14] E.L. Diz, S. Haak, G. Suess-Fink, Z. Beni, G. Laurenczy, Inorg. Synth. 34 (2004) 206.
[15] G. Süss-Fink, S. Haak, V. Ferrand, H. Stœckli-Evans, J. Mol. Catal. A Chem. 143 (1999) 163.
[16] S. Haak, G. Süss-Fink, A. Neels, H. Stœckli-Evans, Polyhedron 18 (1999) 1675.
[17] V.J. Johnston, F.W.B. Einstein, R.K. Pomeroy, J. Am. Chem. Soc. 109 (1987) 7220.
[18] P. Srinivasan, M.E. Tai, W.K. Leong, J. Organomet. Chem. 691 (2006) 941.
[19] M.R. Churchill, J.P. Hutchinson, Inorg. Chem. 17 (1978) 3528.
[20] M.R. Churchill, B.G. DeBoer, Inorg. Chem. 16 (1977) 878.
[21] A.J. Deeming, D.J. Manning, I.P. Rothwell, M.B. Hursthouse, N.P.C. Walker, J. Chem. Soc., Dalton Trans. (1984) 2039.
[22] N.V. Podberezskaya, V.A. Maksakov, I.K. Kedvora, E.D. Kovniets, S.P. Gubin, Koord. Khim. 10 (1984) 919.
[23] A.J. Amoroso, B.F.G. Johnson, J. Lewis, C.K. Li, C.A. Morewood, P.R. Raithby, M.D. Vargas, W.T. Wong, J. Clust. Sci. 6 (1995) 163.
[24] Z. Ahkter, A.J. Edwards, S.L. Ingham, J. Lewis, A.M.M. Castro, P.R. Raithby, G.P. Shields, J. Clust. Sci. 11 (2000) 217.
[25] M. Rahim, K.J. Ahmed, Organometallics 13 (1994) 1751.
[26] Y.-K. Au, K.-K. Cheung, W.-T. Wong, Inorg. Chim. Acta 238 (1995) 193.
[27] A.J. Deeming, R. Peters, M.B. Hursthouse, J.D.C. Backer-Dirks, J. Chem. Soc., Dalton Trans. (1982) 1205.
[28] J.N. Nichrolls, M.D. Vargas, Inorg. Synth. 28 (1990) 232.
[29] C. White, A. Yateo, P.M. Maitlis, D.M. Heinekey, Inorg. Synth. 29 (1992) 228.